Title

A casein kinase 1 prevents expulsion of the oocyte meiotic spindle into a polar body by regulating cortical contractility.

Journal

Molecular biology of the cell, 28(18)

ISSN

1059-1524

Authors

Flynn, Jonathan R
McNally, Francis J

Publication Date

2017-09-01

DOI

10.1091/mbc.e17-01-0056

Peer reviewed

A casein kinase 1 prevents expulsion of the oocyte meiotic spindle into a polar body by regulating cortical contractility

Jonathan R. Flynn and Francis J. McNally*
Department of Molecular and Cellular Biology, University of California, Davis, Davis, CA 95616

ABSTRACT **During female meiosis, haploid eggs are generated from diploid oocytes. This reduction in chromosome number occurs through two highly asymmetric cell divisions, resulting in one large egg and two small polar bodies. Unlike mitosis, where an actomyosin contractile ring forms between the sets of segregating chromosomes, the meiotic contractile ring forms on the cortex adjacent to one spindle pole, then ingresses down the length of the spindle to position itself at the exact midpoint between the two sets of segregating chromosomes. Depletion of casein kinase 1 gamma (CSNK-1) in *Caenorhabditis elegans* led to the formation of large polar bodies that contain all maternal DNA, because the contractile ring ingressed past the spindle midpoint. Depletion of CSNK-1 also resulted in the formation of deep membrane invaginations during meiosis, suggesting an effect on cortical myosin. Both myosin and anillin assemble into dynamic rho-dependent cortical patches that rapidly disassemble in wild-type embryos. CSNK-1 was required for disassembly of both myosin patches and anillin patches. Disassembly of anillin patches was myosin independent, suggesting that CSNK-1 prevents expulsion of the entire meiotic spindle into a polar body by negatively regulating the rho pathway rather than through direct inhibition of myosin.**

Monitoring Editor
Fred Chang
University of California, San Francisco

Received: Jan 23, 2017
Revised: May 25, 2017
Accepted: Jul 5, 2017

INTRODUCTION

Sexually reproducing eukaryotes reduce chromosome ploidy during the process of meiosis to produce haploid gametes. In animals, female meiosis is mediated by meiotic spindles that are asymmetrically positioned with one pole juxtaposed against the oocyte cortex. During anaphase of meiosis I, half the homologous chromosomes are deposited into a first polar body, and during anaphase of meiosis II, half the remaining sister chromatids are deposited into a second polar body. Similar to mitotic cytokinesis, polar body formation requires an actomyosin contractile ring (Maddox *et al.*, 2012). In *Caenorhabditis elegans*, depletion of either actin or nonmuscle myosin II completely blocks both cytokinesis and polar body formation (Shelton *et al.*, 1999). Although mitosis and meiosis use similar cytokinetic machinery, the position of contractile ring formation relative to the spindle drastically differs. During mitosis, the spindle is placed near the center of the cell, and inhibitory signaling from the astral microtubules combined with positive signaling from the spindle midzone allows rho-GTP to accumulate in an equatorial band on the cortex between the sets of segregating chromosomes, which recruits actin and myosin to the site of cytokinesis (Bringmann and Hyman, 2005). Feedback from these two systems keeps the contractile ring positioned between the sets of segregating chromosomes as the ring constricts. In contrast, the meiotic spindle is attached to the cortex by one pole during anaphase and the contractile ring forms on the cortex adjacent to the proximal spindle pole (Maro and Verlhac, 2002; Pielak *et al.*, 2004; Ma *et al.*, 2006; Zhang *et al.*, 2008; Dorn *et al.*, 2010). Either the contractile ring must ingress along the meiotic spindle (Fabritius *et al.*, 2011) or the spindle must move outward through the contractile ring to place the ring between segregating chromosome masses before ring constriction. This suggests that limiting the rate and extent of polar body ring ingression and constriction is essential, as hyperactivation would result in all maternal DNA being expelled into the polar body.

This article was published online ahead of print in MBoC in Press (http://www.molbiolcell.org/cgi/doi/10.1091/mbc.E17-01-0056) on July 12, 2017.

*Address correspondence to: Francis J. McNally (fjmcnally@ucdavis.edu).

Abbreviations used: CK1, casein kinase 1; CSNK-1, casein kinase 1 gamma; DIC, differential interference contrast microscopy; GAP, GTPase-activating protein; GFP, green fluorescent protein; PH, plekstrin homology domain; RNAi, RNA interference.

In *C. elegans*, polar body ring ingression requires the nonmuscle myosin II heavy-chain NMY-2 and the light-chain MLC-5. The velocity of ring ingression is doubled upon depletion of the myosin phosphatase MEL-11 (Fabritius *et al.*, 2011). During meiosis, NMY-2 forms large cortical patches that require the anillin ANI-1, which also forms large cortical patches (Maddox *et al.*, 2005). Similar patches of NMY-2 (Munro *et al.*, 2004) and ANI-1 (Maddox *et al.*, 2005) are also observed after meiosis during polarization of the *C. elegans* zygote and during mitotic cytokinesis. These large myosin patches are not essential, because *C. elegans nop-1* mutants do not form large myosin patches (Tse *et al.*, 2012) but still undergo polar body formation, polarization, and mitotic cytokinesis (Rose *et al.*, 1995). Large cortical patches of myosin or anillin, however, appear to report local concentrations of rho-GTP. rho-GTP is required for polar body formation, polarization, and mitotic cytokinesis and likely mediates all three processes by activating the formin CYK-1 and the myosin-activating rho-kinase LET-502 (Green *et al.*, 2012).

The casein kinase 1 gamma (CSNK-1), one of 78 casein kinase 1 (CK1) homologues in the *C. elegans* genome (Manning, 2005), was identified as a negative regulator of myosin in an RNA interference (RNAi) screen for suppressors of embryonic lethality due to an *nmy-2(ts)* mutation (Fievet *et al.*, 2013). Here we demonstrate that CSNK-1 is a critical negative regulator of the actomyosin network during female meiosis. Depletion of CSNK-1 leads to hypercontractility of the actomyosin network in the meiotic embryo visualized as deep, ectopic membrane invaginations and stabilized cortical patches of both myosin and anillin. In *csnk-1(RNAi)* embryos, the polar body contractile ring ingresses farther down the meiotic spindle than it does in wild-type embryos, occasionally allowing the polar body to capture both sets of segregating chromosomes.

RESULTS

CSNK-1 depletion results in large polar bodies and embryos with a single pronucleus

To examine whether CSNK-1 plays a role in polar body formation during female meiosis, we began by observing pronuclear-stage embryos by differential interference contrast microscopy (DIC). Whereas two small polar bodies were observed on control embryos, *csnk-1(RNAi)* had very large polar bodies (Figure 1A). Polar body size was measured in DIC z-stacks of embryos between pronuclear migration and pronuclear centration as the two-dimensional area of each polar body in the focal plane with the largest area (Figure 1B). Polar body size was significantly greater in *csnk-1(RNAi)* than in controls (26.3 ± 24.3 μm^2 in *csnk-1(RNAi)*, $n = 69$ vs. 4.5 ± 1.3 μm^2 in controls, $n = 53$; two-tailed Student's *t* test $p < 0.0001$) for three different strain backgrounds. Upon further examination of *csnk-1(RNAi)* embryos, we also noticed that there was occasionally only a single pronucleus left in the embryo after the completion of female meiosis. Properly fertilized wild-type embryos should contain two pronuclei after the completion of female meiosis: the female pronucleus and the male pronucleus. Indeed, 50/51 control embryos had two pronuclei and 1/51 control embryos had three pronuclei. In contrast, 12/45 *csnk-1(RNAi)* embryos had a single pronucleus (Figure 1, C and D). The RNAi conditions yielding this 27% frequency of embryos with a single pronucleus caused 44% embryonic lethality. This low level of embryonic lethality is identical to that reported by Panbianco *et al.* (2008) and may indicate incomplete depletion of CSNK-1. These results led to our hypothesis that *csnk-1(RNAi)* embryos form polar bodies that contain all of the maternal DNA.

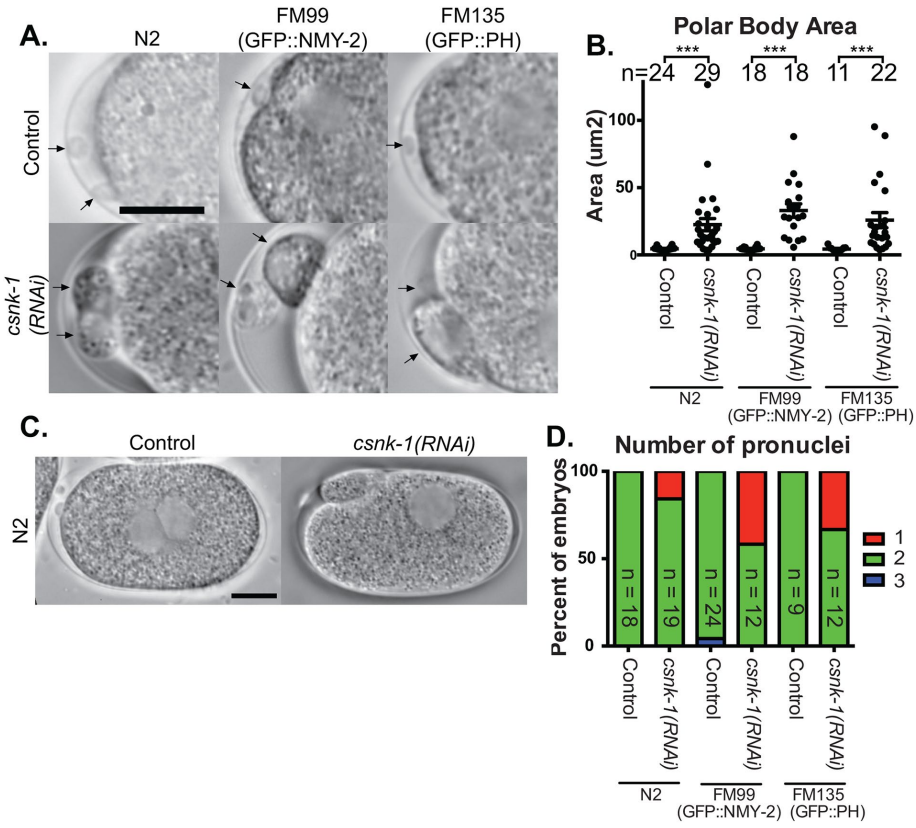

FIGURE 1: CSNK-1 knockdown embryos have large polar bodies and a single pronucleus. (A) DIC images from z-stacks through control vs. *csnk-1(RNAi)* dissected embryos from three different strains (N2, FM99, and FM135). Images were acquired between pronuclear migration and pronuclear breakdown. Arrows mark each visible polar body. Scale bar: 10 μm. (B) Graph of polar body area in N2, FM99, and FM135 control vs. *csnk-1(RNAi)* embryos. Two-dimensional area was measured in the z-stack where the polar body was at its largest size. Statistical analysis was by two-tailed Student's *t* test. ***, $p < 0.001$ (C) Representative images of a control N2 embryo and a *csnk-1(RNAi)* embryo at midfocal plane after pronuclear migration. Scale bar: 10 μm. (D) Graph of the number of pronuclei present in the embryo after female meiosis in control vs. *csnk-1(RNAi)* embryos. The fraction of *csnk-1(RNAi)* embryos with a single pronucleus in the three strain backgrounds tested was not significantly different (Fisher's exact test $p = 0.25$).

CSNK-1 knockdown embryos deposit all maternal DNA into a polar body due to the contractile ring ingressing past 50% spindle length

The single pronucleus in *csnk-1(RNAi)* embryos might be a single female pronucleus in an embryo fertilized by sperm with no DNA (Sadler and Shakes, 2000; Jaramillo-Lambert *et al.*, 2016) or it might be a single male pronucleus formed after extrusion of all the maternal DNA into polar bodies. It is unlikely to be the single female pronucleus of an unfertilized oocyte because these lack an eggshell (Stein and Golden, 2015),

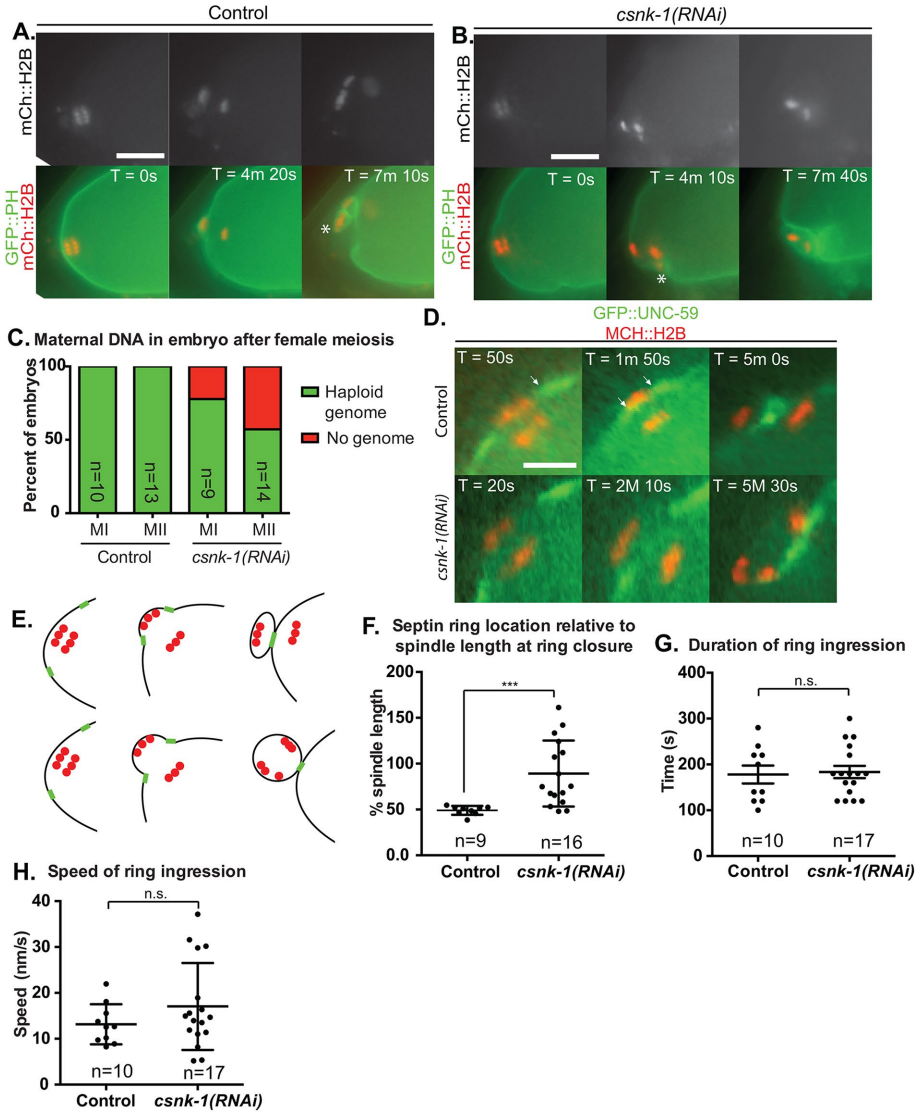

FIGURE 2: CSNK-1 knockdown embryos deposit all maternal DNA into a polar body due to the contractile ring ingressing past 50% spindle length. (A, B) Time-lapse images from a control and a *csnk-1(RNAi)* embryo expressing GFP::PH and mCherry::histone at midfocal plane to show polar body formation. T_0 is one frame after the initiation of chromosome segregation. Asterisks denote the MI polar body when visible. Scale bar: 10 µm. (C) Graph showing the percent of control and *csnk-1(RNAi)* embryos that contain a haploid complement of maternal DNA vs. no maternal DNA after completion of female meiosis. (D) Images from control and *csnk-1(RNAi)* embryos expressing GFP::UNC-59 and mCherry::histone at midfocal plane during polar body formation. T_0 is one frame after the initiation of chromosome segregation. Arrows indicate the inside edge of the contractile ring. Scale bar: 5 µm. (E) Cartoon representation of D with chromosomes in red, UNC-59 in green, and the plasma membrane in black. (F) Location of the contractile ring scission relative to spindle length in control vs. *csnk-1(RNAi)* embryos expressing GFP::UNC-59 and mCherry::histone. (G) Duration of contractile ring ingression in control vs. *csnk-1(RNAi)* embryos expressing GFP::UNC-59 and mCherry::histone between the initiation of contractile ring ingression until contractile ring closure. (H) Speed of contractile ring ingression in embryos expressing GFP::UNC-59 and mCherry::histone measured as the distance between the eggshell and the GFP::UNC-59 signal between the initiation of contractile ring ingression until contractile ring closure. All statistical analysis was by two-tailed Student's *t* test. ***, $p < 0.001$; n.s., not significant.

which is clearly visible in *csnk-1(RNAi)* embryos (Figure 1, A and C). To distinguish between these possibilities, we tracked chromosomes during anaphase in embryos expressing green fluorescent protein (GFP)::plekstrin homology domain (PH) to visualize the plasma membrane and mCherry::histone to visualize the chromosomes. In control embryos, the chromosomes segregated perpendicular to the cortex; then, in late anaphase, the contractile ring ingressed down the meiotic spindle and encapsulated the outer set of chromosomes 10/10 times during anaphase I and 13/13 times during anaphase II (Figure 2, A and C, and Supplemental Video 1). In *csnk-1(RNAi)* embryos, the chromosomes segregated perpendicular to the cortex similar to control embryos 23/23 times, but during late anaphase, the contractile ring ingressed down the entire meiotic spindle, past the inner set of chromosomes, and encapsulated both sets of segregating chromosomes 2/9 times during anaphase I and 6/14 times during anaphase II (Figure 2, B and C). These data show that all maternal DNA was extruded into a polar body in one-third of *csnk-1(RNAi)* embryos, which would result in embryos with a single male pronucleus.

After observing that *csnk-1(RNAi)* embryos frequently deposited all maternal DNA into the polar body despite proper spindle positioning and chromosome segregation, we hypothesized that loss of CSNK-1 might cause misregulation of contractile ring ingression. To accurately determine the location of the contractile ring during polar body formation, we observed embryos expressing GFP::UNC-59 (UNC-59 is a septin that is a component of the contractile ring) and mCherry::histone. In control embryos, GFP:UNC-59 was observed in small patches dispersed around the embryonic cortex. When viewed in the midfocal plane, the meiosis II contractile ring initially appeared as cortical UNC-59 patches near the spindle during anaphase. The contractile ring initially assembled on the cortex with a wide inside diameter of 9.3 ± 0.7 µm (Figure 2D, 50 s). The contractile ring narrowed to 5.5 ± 0.3 µm inside diameter before ingressing down the length of the meiotic spindle (Figure 2D, 1 min, 50 s). Once the contractile ring reached the spindle midpoint, at 50% spindle length, it constricted to sequester the outer set of segregating chromosomes while topologically transforming from a washer to a three-dimensional tube, as described in Dorn *et al*. (2010) (Figure 2, D–F). The contractile ring in *csnk-1(RNAi)* embryos assembled and narrowed on the cortex with diameters similar to controls, starting at 8.3 ± 0.5 µm and narrowing to 5.0 ± 0.3 µm, but ingressed significantly further than 50% spindle length in 12/16 embryos (Figure 2F). The duration of contractile ring ingression, measured as the time between initiation of contractile ring ingression and ring closure, was not significantly different between control and *csnk-1(RNAi)* embryos (Figure 2G). However, a subset of four *csnk-1(RNAi)* embryos

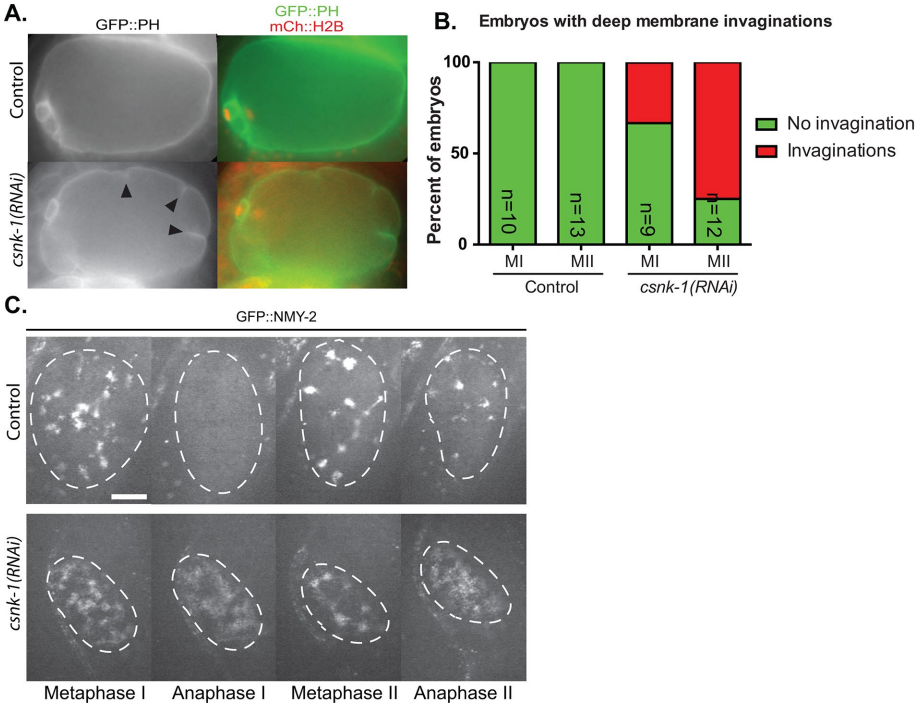

FIGURE 3: CSNK-1 knockdown embryos have ectopic membrane invaginations that correspond with stage-specific changes in cortical myosin during meiosis. (A) Single images of a control and a *csnk-1(RNAi)* embryo expressing GFP::PH and mCherry::histone just after extrusion of the second polar body. Arrowheads indicate deep ectopic membrane invaginations far from the maternal DNA. Scale bar: 10 µm. (B) Graph showing the percent of control and *csnk-1(RNAi)* embryos that display deep (>2 µm) ectopic membrane invaginations greater than 10 µm from the spindle during each stage of meiosis. (C) Images from control and *csnk-1(RNAi)* embryos expressing GFP::NMY-2 to show the cortical myosin network during each stage of meiosis. Scale bar: 10 µm.

exhibited much higher ingression speed than any controls, and three of these four embryos placed both sets of segregating chromosomes in the polar body. In 9/11 *csnk-1(RNAi)* embryos where all maternal DNA was extruded into a polar body, the spindle appeared to change from a perpendicular orientation to a parallel orientation during ring ingression, which may facilitate encapsulation of the spindle by the polar body (Figure 2D, 5 min, 30 s, and Supplemental Video 2). These results suggested that a combination of faster ingression velocity and movement of the spindle into the polar body cause the contractile ring to ingress past the inner set of segregating chromosomes.

CSNK-1 knockdown embryos have ectopic membrane invaginations that correspond with stage-specific changes in cortical myosin during meiosis

Because CSNK-1 is distributed uniformly on the plasma membrane of the entire meiotic embryo (Panbianco *et al.*, 2008) (Supplemental Video 3), we wondered whether the effects of *csnk-1(RNAi)* were limited to the contractile ring region or whether *csnk-1(RNAi)* had a global effect on the plasma membrane. To address this question, we observed a strain expressing GFP::PH (to visualize the plasma membrane) and mCherry::histone (to visualize the chromosomes). In control embryos, deep invaginations of the plasma membrane were restricted to regions where polar body formation is occurring (Figure 3A). In contrast, *csnk-1(RNAi)* embryos had deep ectopic membrane invaginations far from the site of polar body formation in 2/9 embryos during anaphase I and 9/12 embryos during anaphase II (Figure 3, A and B). These ectopic membrane invaginations were deeper (>2 µm) and more stable (>30 s) than previously described shallow invaginations (Fabritius *et al.*, 2011) and pockets caused by cortical granule exocytosis (Bembenek *et al.*, 2007; Fabritius *et al.*, 2011) in wild-type embryos.

The formation of deep, ectopic membrane invaginations far from the meiotic spindle suggested that *csnk-1(RNAi)* may enhance global cortical contractility of the meiotic embryo. To address this, we filmed embryos expressing GFP::NMY-2 (nonmuscle myosin II) and GFP::histone (to track the chromosomes). In nine of nine control embryos, large cortical myosin patches were distributed around the entire embryo during metaphase I. These patches disappeared during anaphase I, then returned during metaphase II and lasted through the completion of female meiosis (Figure 3C). Because midfocal plane images of chromosomes were only captured intermittently, it was impossible to pinpoint the exact time these patches disappeared during anaphase, but it occurred sometime between the initiation of chromosome segregation and formation of the metaphase II plate. In 12/12 *csnk-1(RNAi)* embryos, cortical myosin patches were present during metaphase I as in controls; however, these patches failed to disappear during anaphase I in 11/12 *csnk-1(RNAi)* embryos. The anaphase patches in *csnk-1(RNAi)* embryos expanded in area relative to metaphase patches from 23.6 ± 1.0 µm^2 in metaphase to 44.8 ± 2.7 µm^2 in anaphase; two-tailed Student's *t* test $p < 0.0001$. During metaphase II, *csnk-1(RNAi)* myosin patches were again similar to those in control embryos, but during anaphase II, the patches again expanded (Figure 3C). These data suggested that global changes in cortical myosin activity might be the cause of ectopic, deep membrane invaginations in *csnk-1(RNAi)* embryos.

CSNK-1 knockdown embryos stabilize myosin patches throughout meiosis

The large myosin patches on the cortex of the *C. elegans* pronuclear stage embryo appear to disappear at random (Munro *et al.*, 2004). To analyze the dynamics of these patches, we defined a patch as an area composed of pixels that were at least 5% above the embryo background intensity, and we quantified pixel intensity, patch area, and duration of individual patches during meiosis. *csnk-1(RNAi)* did not affect the average pixel intensity (patch/embryo average ratio: 2.3 ± 1.6 in controls vs. 2.8 ± 1.6 in *csnk-1(RNAi)*) or size of metaphase I cortical myosin patches (23.6 ± 1.2 µm^2 in controls vs. 21.1 ± 1.0 µm^2 in *csnk-1(RNAi)*) (Figure 4, B and C). However, *csnk-1(RNAi)* significantly increased the duration of cortical myosin patches from an average of 73.6 ± 33.2 s in control embryos ($n = 95$) to an average of 291.3 ± 139.1 s in *csnk-1(RNAi)* embryos ($n = 84$); two-tailed Student's *t* test $p < 0.0001$ (Figure 4D). The patches in *csnk-1(RNAi)* often lasted through multiple stages of meiosis, so patches were only categorized into either meiosis I or meiosis II. These data indicate that CSNK-1 has a specific role in myosin patch disassembly throughout meiosis.

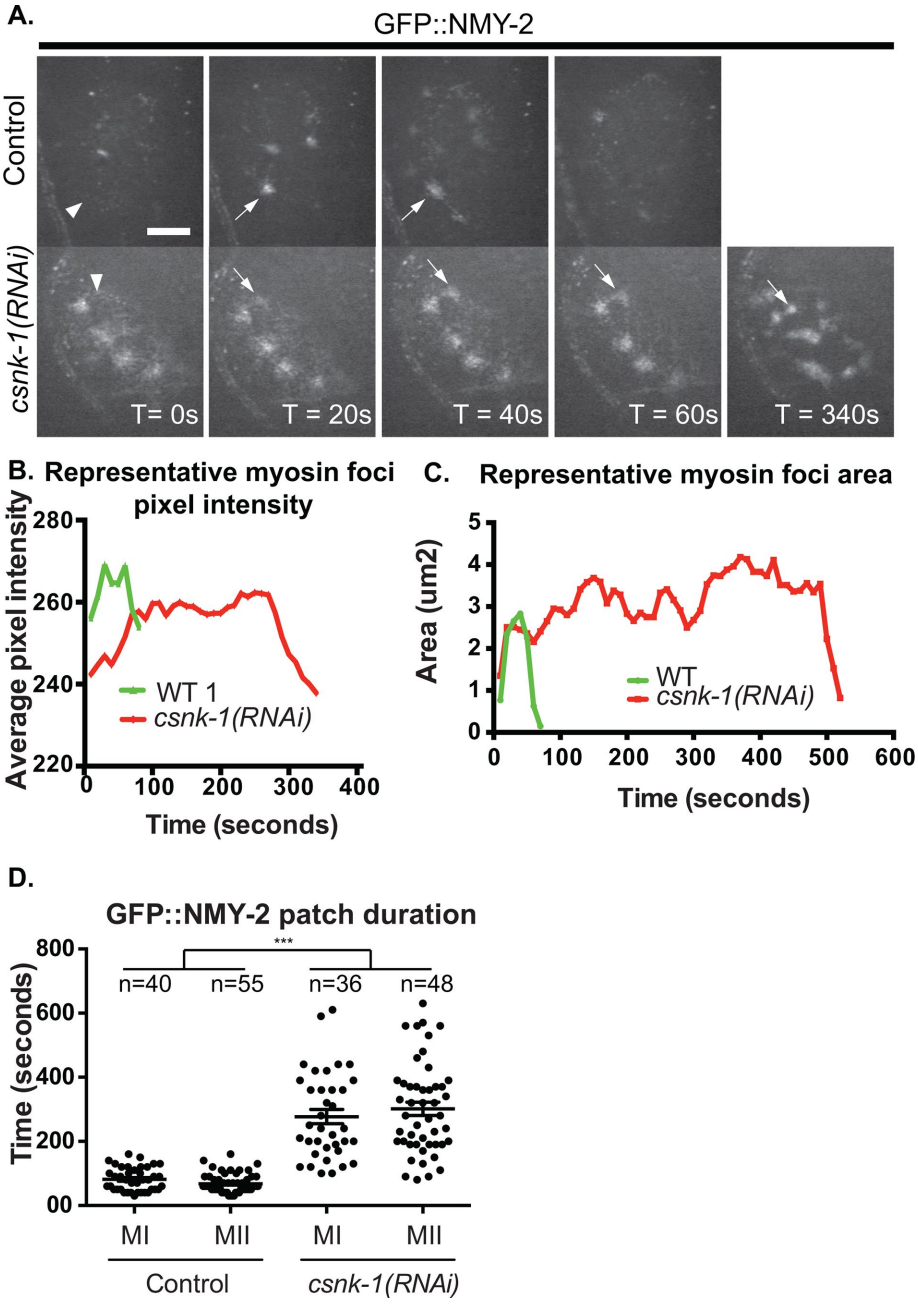

FIGURE 4: CSNK-1 knockdown stabilizes myosin patches throughout meiosis. (A) Images from a control and a *csnk-1(RNAi)* embryo expressing GFP::NMY-2 during meiosis I. The arrowhead denotes where the patch will form, and the arrows follow the patch over time. Scale bar: 10 µm. (B, C) Representative graphs of an individual control myosin patch compared with an individual *csnk-1(RNAi)* myosin patch measuring average pixel intensity and size over time, respectively. (D) Graph showing cortical myosin patch duration in control and *csnk-1(RNAi)* embryos, further categorized into meiosis I and meiosis II. Each point represents the duration of a single myosin patch. In each condition, four to five unique patches were measured in 10 different embryos. Statistical analysis was by two-tailed Student's *t* test. ***, $p < 0.001$.

CSNK-1 is a negative regulator of rho-GTP rather than a negative regulator of myosin

The deep membrane invaginations and altered kinetics of cortical myosin patches observed in *csnk-1(RNAi)* meiotic embryos suggested that CSNK-1 regulates myosin activity, but it remained unclear whether this was through a direct or indirect interaction. To address this, we identified potential targets of CSNK-1 by looking for consensus CK1 sites in myosin and proteins demonstrated to regulate myosin in the *C. elegans* zygote. We found three potential targets with consensus CK1 sites in the *C. elegans* phosphorylation databases (Bodenmiller *et al.*, 2008; Gnad *et al.*, 2011): RGA-3/4 (the major GTPase-activating protein [GAP] for rho), MEL-11 (myosin phosphatase), and NMY-2 (myosin heavy chain). Of these targets, mass spectrometry analysis showed both MEL-11 and NMY-2 had phosphorylated CK1 sites in vivo in *C. elegans*. No CK1 phosphorylations have yet been identified in vivo in *C. elegans* RGA-3/4; however, RGA-3/4 homologues are phosphorylated on CK1 sites in HeLa cells (Gnad *et al.*, 2011). To narrow down the potential targets of CSNK-1, we first looked at polar body size in *rga-3/4(RNAi)* and *mel-11(it26)* embryos, hypothesizing that loss of a downstream target that is positively regulated by CSNK-1 would cause large polar bodies similar to *csnk-1(RNAi)* (Figure 5A). We could not test *nmy-2(RNAi)*, because depletion of *nmy-2* abolishes polar body formation. *rga-3/4(RNAi)* embryos often produced large polar bodies, while *mel-11(it26)* embryos produced small polar bodies similar to control embryos (Figure 5, A and B). We next looked at the number of pronuclei remaining in the embryo after meiosis, again hypothesizing that depletion of the downstream target of CSNK-1 would generate embryos with a single pronucleus after the completion of meiosis similar to *csnk-1(RNAi)* embryos (Figure 5C). *rga-3/4(RNAi)* embryos occasionally had a single pronucleus left after meiosis, while *mel-11(it26)* embryos always had two pronuclei (Figure 5, C and D). Together these results suggested that RGA-3/4 might be acting in the same pathway as CSNK-1, but MEL-11 is not. RGA-3/4 is thought to convert rho-GTP to rho-GDP, whereas MEL-11 is thought to inhibit myosin directly by removing activating phosphates from the MLC-4 regulatory light chain. Thus our results suggested that CSNK-1 might be an inhibitor of rho-GTP production rather than a direct inhibitor of myosin.

To further test the idea that CSNK-1 regulates rho-GTP, we monitored cortical rho dynamics, hypothesizing that proteins acting upstream of rho would affect cortical rho residency at the cortex, whereas proteins acting downstream of rho would not. Because rho-GTP recruits anillin to the cortex (Piekny and Glotzer, 2008), we observed embryos expressing GFP::ANI-1, as an indirect method to visualize active rho, and mCherry::histone to track the chromosomes. Similar to the myosin patches, transient anillin patches appeared on the cortex in a seemingly random manner (Figure 6A). We measured individual anillin patches over time during meiosis II by thresholding and quantifying

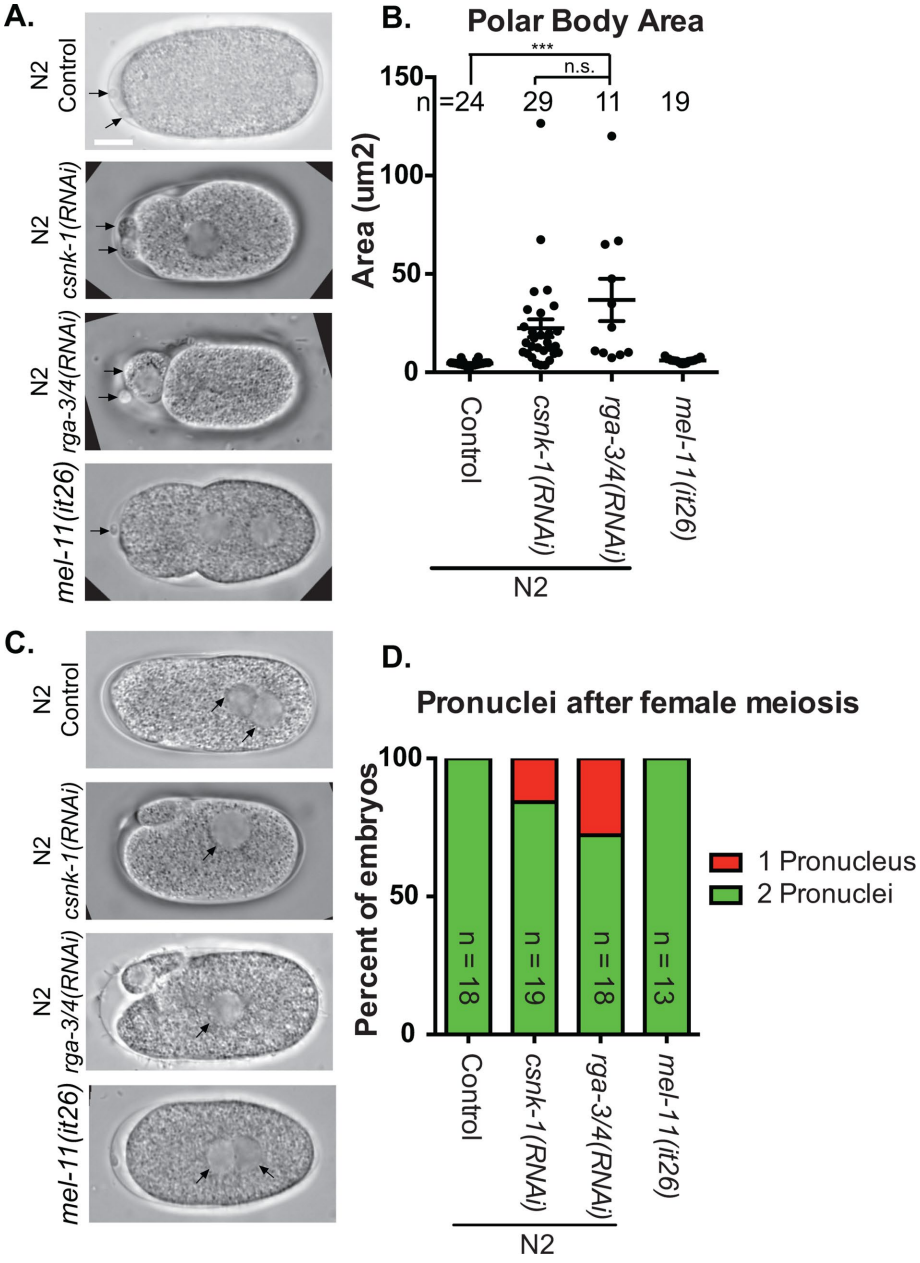

FIGURE 5: rho-GAP knockdown phenocopies CSNK-1 knockdown. (A) DIC images from z-stacks through control, *csnk-1(RNAi)*, *rga-3/4(RNAi)*, and *mel-11(it26)* dissected embryos. Images were acquired between pronuclear migration and pronuclear breakdown. Arrows mark each visible polar body. Scale bar: 10 µm. (B) Graph of polar body area in control, *csnk-1(RNAi)*, *rga-3/4(RNAi)*, and *mel-11(it26)* embryos. Two-dimensional area was measured in the z-stack where the polar body was at its largest size. (C) Representative images of control, *csnk-1(RNAi)*, *rga-3/4(RNAi)*, and *mel-11(it26)* embryos at midfocal plane after pronuclear migration. Arrows indicate each nucleus. Scale bar: 10 µm. (D) Graph of the number of pronuclei present in the embryo after female meiosis in control, *csnk-1(RNAi)*, *rga-3/4(RNAi)*, and *mel-11(it26)* embryos. Statistical analysis was by two-tailed Student's *t* test. ***, $p < 0.001$; n.s., not significant.

patches that were 5% brighter than the average embryo fluorescence. Anillin patches in control embryos were short-lived, lasting only 95.5 ± 6.2 s (Figure 6, A and B), similar to the duration of myosin patches. *csnk-1(RNAi)* resulted in a significant increase in cortical anillin patch residency time, with patches persisting 360.5 ± 54.7 s ($p < 0.0001$). Although rho and anillin act upstream of myosin, feedback from myosin to anillin remained a possibility. If CSNK-1 directly phosphorylated myosin, this phosphorylation would have to be inhibitory in order to explain the hypercontractile phenotype of *csnk-1(RNAi)*. In this scenario, increased myosin activity would have to prolong the lifetime of anillin patches, and a decrease in myosin activity would be expected to shorten the lifetime of anillin patches. In contradiction with this prediction, anillin patch duration in *nmy-2(RNAi)* was slightly prolonged, lasting 130.2 ± 7.9 s ($p < 0.001$). *nmy-2(RNAi)* did appear to slightly increase anillin cortical patch residency time, but not nearly as significantly as *csnk-1*. We expected to see increased anillin patch duration in *rga-3/4(RNAi)*; however, we instead saw an overall enrichment of anillin on the cortex during metaphase II and anaphase II in 10/10 embryos (Figure 6A). Together these data suggested that CSNK-1 acts upstream of rho, possibly on RGA-3/4, rather than directly on myosin.

To further test this hypothesis, we monitored the duration of cortical patches of GFP:AHPH, a truncation of ANI-1 that contains only the anillin homology domain and the membrane-targeting PH. This fusion protein has been used extensively as a probe for rho-GTP (Tse *et al.*, 2012; Nishikawa *et al.*, 2017), and its dynamics are unaffected by myosin depletion (Nishikawa *et al.*, 2017). GFP:AHPH cortical patches had a duration of 71.4 ± 3.8 s in control embryos and 425.8 ± 38.7 s in *csnk-1(RNAi)* embryos during meiosis (Figure 6C). This result strongly indicates that CSNK-1 acts upstream of myosin on the rho-GTP pathway.

csnk-1(RNAi) had a weaker effect on cortical anillin than *rga-3/4(RNAi)*, which correlated with the embryonic lethality, which was higher for *rga-3/4(RNAi)* than for *csnk-1(RNAi)* (45% for *csnk-1*; 100% for *rga-3/4*). Either CSNK-1 is not absolutely required for RGA-3/4 activity or CSNK-1 is not fully depleted by RNAi in our experiments. To address this, we analyzed the progeny from worms heterozygous for *tm1762*, a deletion allele of *csnk-1*, and hT2, a balancer composed of a reciprocal translocation bearing a recessive lethal mutation and a GFP transgene expressed in the pharynx. Among the viable L3-adult progeny of a control *dpy-5 unc-13/hT2* strain, 34/156 were non-GFP and dpy unc (result from 10 broods and >1000 total progeny). Among the viable L3-adult progeny of *csnk-1(tm1762)/hT2*, 0/489 were non-GFP (result from 10 broods and >1000 progeny). This result indicates that 100% of *csnk-1(tm1762)* homozygotes either do not hatch or do not develop past the L1 stage. Because the 55% of *csnk-1(RNAi)* progeny that hatched all developed into adults, we conclude that CSNK-1 protein is only partially depleted by RNAi.

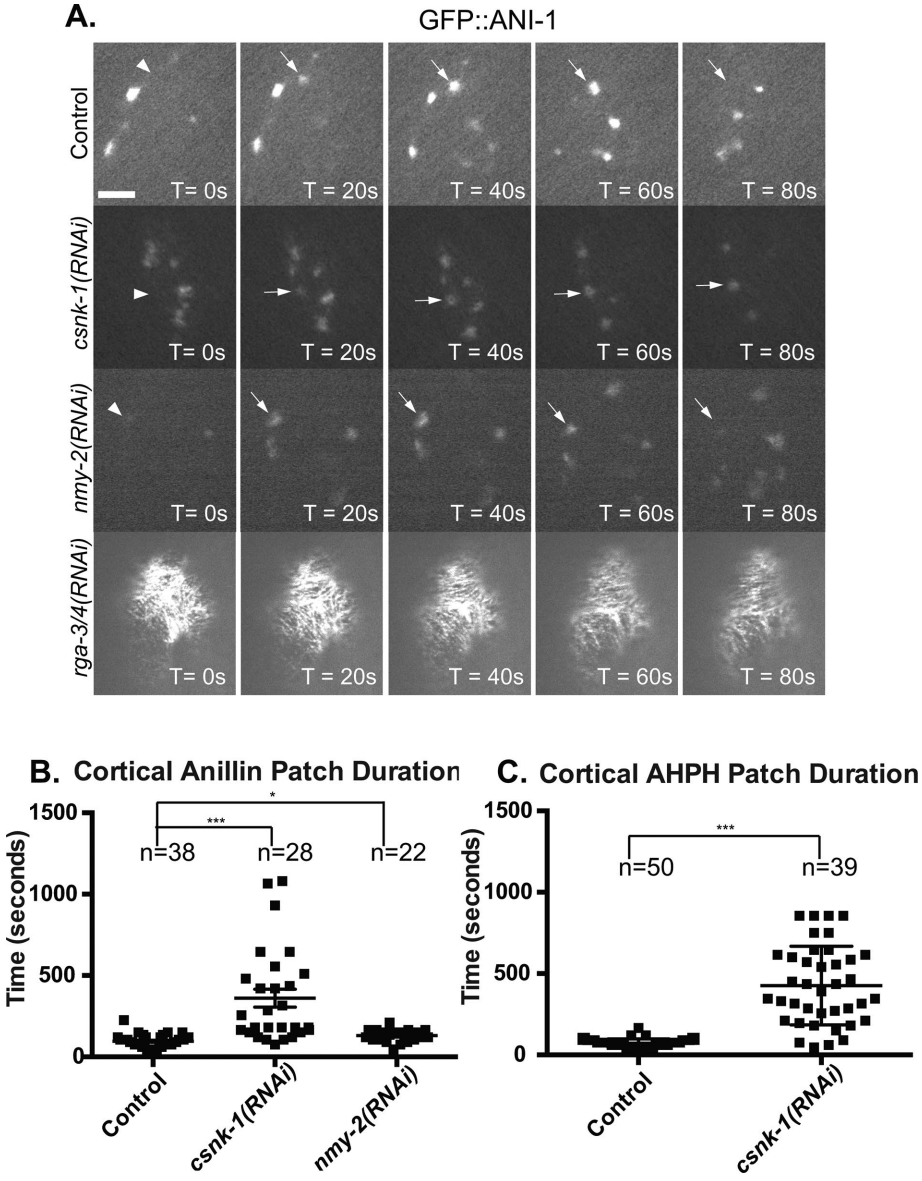

FIGURE 6: CSNK-1 knockdown stabilizes rho-GTP cortical patches. (A) Time-lapse images from of *csnk-1(RNAi)*, *nmy-2(RNAi)*, and *rga-3(RNAi)* embryos expressing GFP::ANI-1 during meiosis II. Cell cycle time was determined from mCherry::histone images in a deeper focal plane. The arrowhead denotes where the patch will form, and the arrows follow the patch over time. Scale bar: 10 µm. (B) Graph showing cortical GFP:ANI-1 patch duration in control, *csnk-1(RNAi)*, *and nmy-2(RNAi)* embryos. Each point represents the duration of a single anillin patch. In each condition, four to five unique patches were measured in 10 different embryos.(C) Graph showing cortical GFP:AHPH patch duration in control, *csnk-1(RNAi)*, *and nmy-2(RNAi)* embryos. Each point represents the duration of a single anillin patch. In each condition, four to five unique patches were measured in 10 different embryos. Statistical analysis was by two-tailed Student's *t* test. *, $p < 0.001$, ***, $p < 0.0001$.

DISCUSSION

The presence of large polar bodies, such as those observed upon *csnk-1* depletion, has been associated with failures in katanin-dependent bipolar spindle assembly (Mains *et al.*, 1990) and dynein-dependent meiotic spindle positioning (van der Voet *et al.*, 2009) and defects in the actomyosin-based polar body contractile ring (Dorn *et al.*, 2010; Fabritius *et al.*, 2011). CSNK-1 has previously been linked to both dynein-dependent spindle positioning and the actomyosin network. *csnk-1(RNAi)* embryos exhibit excessive pronuclear and mitotic spindle movements that depend on the dynein regulator LIN-5 (Panbianco *et al.*, 2008). LIN-5 is also required for rotation of the meiotic spindle to the perpendicular orientation just before polar body formation (van der Voet *et al.*, 2009). However, we found that meiotic spindle rotation occurred normally in *csnk-1(RNAi)* embryos, suggesting that the large polar bodies in *csnk-1(RNAi)* embryos are not due to defects in dynein-dependent spindle positioning. *csnk-1(RNAi)* embryos were also reported to have excessively deep myosin-dependent pseudocleavage furrows during pronuclear migration, and this phenotype was LIN-5 independent (Panbianco *et al.*, 2008). *csnk-1(RNAi)* was also shown to rescue *nmy-2(ts)* lethality (Fievet *et al.*, 2013), further suggesting that CSNK-1 is a negative regulator of NMY-2. Through time-lapse imaging we showed that *csnk-1(RNAi)* causes the formation of deep membrane invaginations throughout the meiotic embryo. This phenotype suggests that CSNK-1 acts as a negative regulator of global myosin contractility during meiosis.

There is a hierarchy to contractile ring and cortical myosin patch assembly that begins with the rho-GEF ECT-2 and the rho-GAP's RGA-3/4 controlling the nucleotide state of rho. Cortical rho-GTP is able to recruit ANI-1, which subsequently recruits NMY-2 (Yuce *et al.*, 2005; Motegi and Sugimoto, 2006; Dorn *et al.*, 2010; Tse *et al.*, 2012). Therefore, if CSNK-1 acted as a direct inhibitor of NMY-2, *csnk-1(RNAi)* would not be expected to affect GFP:ANI-1 cortical patches. We found that both *rga-3/4(RNAi)* and *csnk-1(RNAi)* significantly stabilized cortical ANI-1, whereas *nmy-2(RNAi)* had only a minor effect on ANI-1 patch stability. This result strongly suggested that CSNK-1 promotes myosin patch disassembly by negatively regulating rho-GTP, possibly by activating RGA-3/4, rather than by directly inhibiting NMY-2.

In *C. elegans*, the contractile ring forms on the cortex near the meiotic spindle, significantly narrows in diameter, and then ingresses down the meiotic spindle. Once the contractile ring reaches the spindle midpoint, it begins to close while changing shape from a washer to a three-dimensional tube structure before scission, which occurs on the embryo side of the tube, leaving a visible midbody remnant in the polar body (Dorn *et al.*, 2010; Cortes *et al.*, 2015) (Figure 7). The transformation of the contractile machinery from a washer to a tube requires the anillin ANI-1. In *ani-1(RNAi)*, the contractile machinery remained in a washer and eventually failed to complete scission (Dorn *et al.*, 2010). This suggests that the transformation of the cytokinetic machinery from a washer to a tube may help facilitate scission. Contractile ring scission still occurs at the spindle midpoint in *mel-11(RNAi)*, where the contractile ring ingression

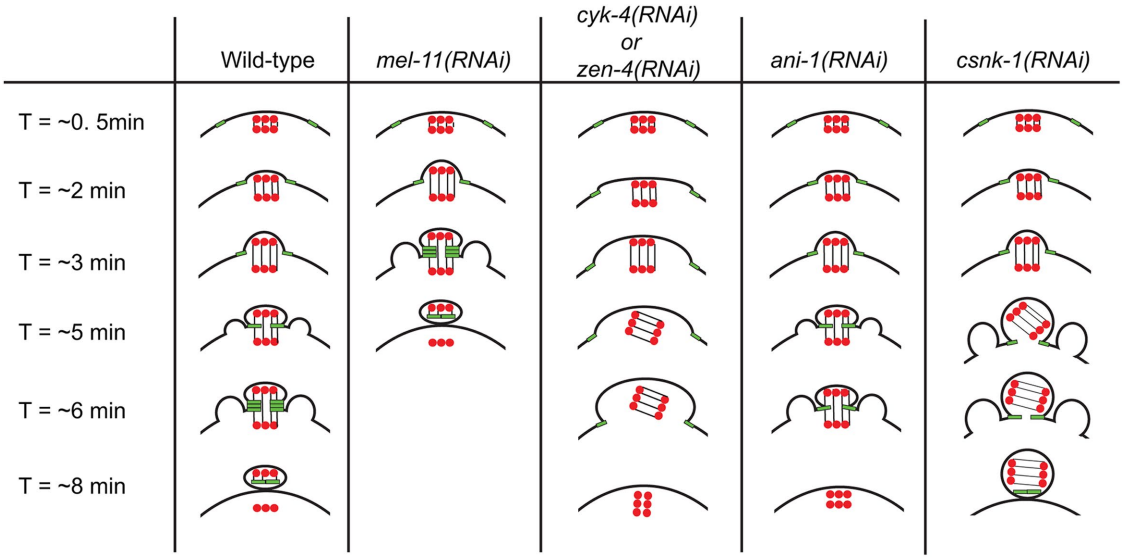

FIGURE 7: Overview of known polar body defects. Sequential events of polar body formation in wild type, *mel-11(RNAi)*, *cyk-4(RNAi)*, *zen-4(RNAi)*, *ani-1(RNAi)*, and *csnk-1(RNAi)* emphasizing known defects. Red circles represent chromosomes, while green blocks represent cytokinetic machinery. Black lines indicate microtubule bundles. Times are relative to spindle rotation.

velocity is doubled, and in a katanin mutant, where the spindle is significantly longer, suggesting there is a signal on the spindle that informs the contractile ring to complete scission (Fabritius *et al.*, 2011). In centralspindlin knockdowns, *cyk-4(RNAi)* or *zen-4(RNAi)*, the contractile ring is established with a wide diameter but never narrows, causing ingression of a wide contractile ring that ultimately fails to form a polar body (Fabritius *et al.*, 2011). This suggests a narrow contractile ring is necessary to communicate with the meiotic spindle to complete scission. Curiously, *csnk-1(RNAi)* embryos form polar bodies containing all maternal DNA, despite having a narrow contractile ring during ingression and failure to transform the cytokinetic machinery from a washer to a three-dimensional tube. Anillin is present in *csnk-1(RNAi)* and may still localize to the cleavage furrow to assist in scission. The cytokinetic machinery failed to transform from a washer to a tube during scission in *csnk-1(RNAi)*, suggesting that the three-dimensional tube might not be necessary to complete scission but instead is a product of a spindle midzone being present as a scaffold. This scaffold is not present in *csnk-1(RNAi)* embryos, because the spindle midzone is entirely in the polar body. Alternatively, the three-dimensional tube may be required to generate enough force to complete scission only when there is a spindle inserted through the polar body ring. Additionally, *csnk-1(RNAi)* must have an additional defect in communication between the contractile ring and the meiotic spindle that allows the contractile ring to push past the entire spindle.

rho-GTP-dependent, dynamic cortical patches of myosin and anillin have been reported in several species and cell types (Munro *et al.*, 2004; Martin *et al.*, 2009; He *et al.*, 2010; Tse *et al.*, 2012; Bement *et al.*, 2015; Baird *et al.*, 2016), but their function is unknown. Work in *Xenopus* and starfish oocytes has suggested a myosin-independent oscillator in which patches appear and grow because rho-GTP recruits more rho-GTP, then patches shrink and disappear because rho-GTP promotes local actin polymerization and F-actin drives rho-GTP back to rho-GDP (Bement *et al.*, 2015). *C. elegans* ANI-1 has a myosin-binding domain and a rho-GTP–binding domain (Maddox *et al.*, 2005). Previous work demonstrated that meiotic ANI-1 cortical patches assemble in the absence of myosin (Maddox *et al.*, 2005), and we have shown here that ANI-1 patch disassembly is only minimally affected by myosin depletion. Thus, during *C. elegans* meiosis, cortical patches of myosin and anillin may also report on myosin-independent oscillations of rho-GTP. Here we observed that large myosin patches are not present during *C. elegans* meiotic anaphase I when ingression of the first polar body is occurring but are present during metaphase I and II when furrowing is suppressed. Thus the precise relationship between the apparent rho oscillator and polar body ring ingression remains to be elucidated.

MATERIALS AND METHODS

C. elegans strains

The following strains were used: N2, FM99: created by crossing *unc-119(ed3)III; zuIs45 [nmy-2::NMY-2::GFP;unc-119(+)]* V (Nance *et al.*, 2003) with *ruIs32 [pie-1::GFP::H2B + unc-119(+)] III* (Praitis *et al.*, 2001); FM135: *ltIs37 [(pAA64) pie-1p::mCherry::his-58 + unc-119(+)] IV; ltIs38 [pAA1; pie-1::GFP::PH(PLC1delta1) + unc-119(+)]*; FM317: *unc-119(ed3) III; ltIs28 [pASM14; pie-1/GFP-TEV-STag::ani-1; unc-119 (+)]; ltIs37 [pAA64; pie-1/mCherry::his-58)*; KK332: *mel-11(it26) unc-4(e120) sqt-1(sc13)/mnC1 dpy-10(e128) unc-52(e444) II*; FM312: *ltIs37 [(pAA64) pie-1p::mCherry::his-58 + unc-119(+)]; ltIs20 [pASM10; pie-1/GFP::unc-59; unc-119 (+)]ltIs44 [pAA173; pie-1/mCherry::PH(PLC1delta1); unc-119(+)]*; FM421: made by crossing MG636: *mgSi5[cb-UNC-119 (+) GFP::ANI-1(AH+PH)]II* with OD57: *ltIs37 [(pAA64) pie-1p::mCherry::his-58 + unc-119(+)] IV*, WM149: *dpy-5(e61) unc-13(e51) I/hT2 [bli-4(e937) let-?(q782) qIs48] (I;III), csnk-1(tm1762)/ hT2 [bli-4(e937) let-?(q782) qIs48] (I;III)* (provided by the MITANI Lab through the National Bio-Resource Project of the MEXT, Japan).

Live imaging

In utero time lapse: adult hermaphrodite worms were anesthetized as previously described (Kirby *et al.*, 1990; McCarter *et al.*, 1999)

and mounted between a 22 × 30 mm coverslip and a thin 3% agarose pad on a slide (Figures 2, A and B, 3C, 4A, and 6A). Ex utero time lapse: adult hermaphrodite worms were placed in 10 µl of 0.8X egg salts (1× egg salts: 118 mM NaCl, 40 mM KCl, 3.4 mM $MgCl_2$, 3.4 mM $CaCl_2$, and 5 mM HEPES, pH 7.4; Carvalho *et al.*, 2011) on a 22 × 30 mm coverglass where the embryos were dissected out and the remaining worm carcasses were carefully removed. The coverslip was then inverted onto a slide that had coverslips attached as spacers to prevent squashing the embryos (Figures 1, A and C, 2D, and 5, A and C). Images in Figures 2D, 3C, and 4A were captured with a PerkinElmer-Cetus Ultraview Spinning Disk Confocal equipped with an Orca R2 CCD and an Olympus 100×/NA 1.35 oil objective. Images in Figures 1, A and C, 2, A and B, and 5, A and C) were captured with an Olympus IX71 inverted microscope with a 60×/NA 1.42 Plan-Apo objective and equipped with a Hamamatsu Orca R2 C10600-10B digital CCD camera. Images in Figure 6A were captured with a PerkinElmer-Cetus Ultraview Spinning Disk Confocal equipped with an ORCA Flash 4.0 CMOS camera and an Olympus 100×/NA1.35 oil objective.

RNAi by feeding

All of the RNAi experiments were performed by feeding bacteria (HT115) induced to express double-stranded RNA corresponding to each gene (Kamath *et al.*, 2001; Timmons *et al.*, 2001). The bacterial strains used (*csnk-1*, *rga-3/4*, and *nmy-2*) were obtained from the Ahringer feeding library (Kamath *et al.*, 2003). L3/4 hermaphrodite worms were fed on *rga-3/4* for ~30 h or *nmy-2* bacteria for ~48 h at 20°C. L1 hermaphrodite worms were fed on *csnk-1* bacteria for ~72 h at 20°C. The specificity of *csnk-1(RNAi)* has previously been demonstrated by transgene rescue (Panbianco *et al.*, 2008). Hatch counts were compared with control worms on an empty vector feeding strain, and all resulted in increased lethality compared with control. *rga-3/4(RNAi)* was ~100% lethal after 30 h; *nmy-2(RNAi)* was 100% lethal after 48 h; *csnk-1(RNAi)* was ~15% lethal after 24 h, ~30% lethal after 48 h, and ~45% lethal after 72 h.

Measurements and quantification

Polar body size was measured on z-stacks through embryos in DIC. The two-dimensional area was measured in the frame where the polar body appeared the largest. Contractile ring ingression speed, ring closure %, and ingression duration were all measured from time-lapse image sequences of embryos during chromosome segregation. Patches of GFP:NMY-2 and GFP:ANI-1 were defined with a threshold 5% higher than the average pixel intensity of an embryo, and patch lifetimes were measured with an ImageJ script.

ACKNOWLEDGMENTS

We thank Daniel Cortes for assistance writing the ImageJ script used for patch lifetime measurements and Kari Price, Lesilee Rose, and Karen McNally for initial observations of large polar bodies on *csnk-1(RNAi)* embryos. We thank Dan Starr, Bo Liu, and Karen McNally for critical reading of the article. We thank Amy Shaub-Maddox, Karen Oegema, the MITANI Lab (National Bio-Resource Project of the MEXT, Japan), and the *Caenorhabditis* Genetics Center, which is funded by the National Institutes of Health Office of Research Infrastructure Programs (P40 OD010440), for strains. This work was supported by National Institute of General Medical Sciences grant 1R01GM-079421 and U.S. Department of Agriculture National Institute of Food and Agriculture Hatch project 1009162 (to F.J.M.).

REFERENCES

Baird MA, Billington N, Wang A, Adelstein RS, Sellers JR, Fischer RS, Waterman CM (2016). Local pulsatile contractions are an intrinsic property of the myosin 2A motor in the cortical cytoskeleton of adherent cells. Mol Biol Cell 28, 240–251.

Bembenek JN, Richie CT, Squirrell JM, Campbell JM, Eliceiri KW, Poteryaev D, Spang A, Golden A, White JG (2007). Cortical granule exocytosis in *C. elegans* is regulated by cell cycle components including separase. Development 134, 3837–3848.

Bement WM, Leda M, Moe AM, Kita AM, Larson ME, Golding AE, Pfeuti C, Su KC, Miller AL, Goryachev AB, von Dassow G (2015). Activator-inhibitor coupling between Rho signalling and actin assembly makes the cell cortex an excitable medium. Nat Cell Biol 17, 1471–1483.

Bodenmiller B, Campbell D, Gerrits B, Lam H, Jovanovic M, Picotti P, Schlapbach R, Aebersold R (2008). PhosphoPep—a database of protein phosphorylation sites in model organisms. Nat Biotechnol 26, 1339–1340.

Bringmann H, Hyman AA (2005). A cytokinesis furrow is positioned by two consecutive signals. Nature 436, 731–734.

Carvalho A, Olson SK, Gutierrez E, Zhang K, Noble LB, Zanin E, Desai A, Groisman A, Oegema K (2011). Acute drug treatment in the early *C. elegans* embryo. PLoS One 6, e24656.

Cortes DB, McNally KL, Mains PE, McNally FJ (2015). The asymmetry of female meiosis reduces the frequency of inheritance of unpaired chromosomes. Elife 4, e06056.

Dorn JF, Zhang L, Paradis V, Edoh-Bedi D, Jusu S, Maddox PS, Maddox AS (2010). Actomyosin tube formation in polar body cytokinesis requires anillin in *C. elegans*. Curr Biol 20, 2046–2051.

Fabritius AS, Flynn JR, McNally FJ (2011). Initial diameter of the polar body contractile ring is minimized by the centralspindlin complex. Dev Biol 359, 137–148.

Fievet BT, Rodriguez J, Naganathan S, Lee C, Zeiser E, Ishidate T, Shirayama M, Grill S, Ahringer J (2013). Systematic genetic interaction screens uncover cell polarity regulators and functional redundancy. Nat Cell Biol 15, 103–112.

Gnad F, Gunawardena J, Mann M (2011). PHOSIDA 2011: the posttranslational modification database. Nucleic Acids Res 39, D253–D260.

Green RA, Paluch E, Oegema K (2012). Cytokinesis in animal cells. Annu Rev Cell Dev Biol 28, 29–58.

He L, Wang X, Tang HL, Montell DJ (2010). Tissue elongation requires oscillating contractions of a basal actomyosin network. Nat Cell Biol 12, 1133–1142.

Jaramillo-Lambert A, Fabritius AS, Hansen TJ, Smith HE, Golden A (2016). The identification of a novel mutant allele of topoisomerase II in *Caenorhabditis elegans* reveals a unique role in chromosome segregation during spermatogenesis. Genetics 204, 1407–1422.

Kamath RS, Fraser AG, Dong Y, Poulin G, Durbin R, Gotta M, Kanapin A, Le Bot N, Moreno S, Sohrmann M, Welchman DP, Zipperlen P, Ahringer J (2003). Systematic functional analysis of the *Caenorhabditis elegans* genome using RNAi. Nature 421, 231–237.

Kamath RS, Martinez-Campos M, Zipperlen P, Fraser AG, Ahringer J (2001). Effectiveness of specific RNA-mediated interference through ingested double-stranded RNA in *Caenorhabditis elegans*. Genome Biol 2, RESEARCH0002.

Kirby C, Kusch M, Kemphues K (1990). Mutations in the *par* genes of *Caenorhabditis elegans* affect cytoplasmic reorganization during the first cell cycle. Dev Biol 142, 203–215.

Ma C, Benink HA, Cheng D, Montplaisir V, Wang L, Xi Y, Zheng PP, Bement WM, Liu XJ (2006). Cdc42 activation couples spindle positioning to first polar body formation in oocyte maturation. Curr Biol 16, 214–220.

Maddox AS, Azoury J, Dumont J (2012). Polar body cytokinesis. Cytoskeleton (Hoboken) 69, 855–868.

Maddox AS, Habermann B, Desai A, Oegema K (2005). Distinct roles for two *C. elegans* anillins in the gonad and early embryo. Development 132, 2837–2848.

Mains PE, Kemphues KJ, Sprunger SA, Sulston IA, Wood WB (1990). Mutations affecting the meiotic and mitotic divisions of the early *Caenorhabditis elegans* embryo. Genetics 126, 593–605.

Manning G (2005). Genomic overview of protein kinases. In: WormBook, ed. C. elegans Research Community. doi: 10.1895/wormbook.1.60.1.

Maro B, Verlhac MH (2002). Polar body formation: new rules for asymmetric divisions. Nat Cell Biol 4, E281–E283.

Martin AC, Kaschube M, Wieschaus EF (2009). Pulsed contractions of an actin-myosin network drive apical constriction. Nature 457, 495–499.

McCarter J, Bartlett B, Dang T, Schedl T (1999). On the control of oocyte meiotic maturation and ovulation in *Caenorhabditis elegans*. Dev Biol 205, 111–128.
Motegi F, Sugimoto A (2006). Sequential functioning of the ECT-2 RhoGEF, RHO-1 and CDC-42 establishes cell polarity in *Caenorhabditis elegans* embryos. Nat Cell Biol 8, 978–985.
Munro E, Nance J, Priess JR (2004). Cortical flows powered by asymmetrical contraction transport PAR proteins to establish and maintain anterior-posterior polarity in the early *C. elegans* embryo. Dev Cell 7, 413–424.
Nance J, Munro EM, Priess JR (2003). *C. elegans* PAR-3 and PAR-6 are required for apicobasal asymmetries associated with cell adhesion and gastrulation. Development 130, 5339–5350.
Nishikawa M, Naganathan SR, Jülicher F, Grill SW (2017). Controlling contractile instabilities in the actomyosin cortex. Elife 6, e19595.
Panbianco C, Weinkove D, Zanin E, Jones D, Divecha N, Gotta M, Ahringer J (2008). A casein kinase 1 and PAR proteins regulate asymmetry of a PIP(2) synthesis enzyme for asymmetric spindle positioning. Dev Cell 15, 198–208.
Piekny AJ, Glotzer M (2008). Anillin is a scaffold protein that links RhoA, actin, and myosin during cytokinesis. Curr Biol 18, 30–36.
Pielak R, Gaysinskaya VA, Cohen WD (2004). Formation and function of the polar body contractile ring in *Spisula*. Dev Biol 269, 421–432.
Praitis V, Casey E, Collar D, Austin J (2001). Creation of low-copy integrated transgenic lines in *Caenorhabditis elegans*. Genetics 157, 1217–1226.
Rose LS, Lamb ML, Hird SN, Kemphues KJ (1995). Pseudocleavage is dispensable for polarity and development in *C. elegans* embryos. Dev Biol 168, 479–489.
Sadler PL, Shakes DC (2000). Anucleate *Caenorhabditis elegans* sperm can crawl, fertilize oocytes and direct anterior-posterior polarization of the 1-cell embryo. Development 127, 355–366.
Shelton CA, Carter JC, Ellis GC, Bowerman B (1999). The nonmuscle myosin regulatory light chain gene mlc-4 is required for cytokinesis, anterior-posterior polarity, and body morphology during *Caenorhabditis elegans* embryogenesis. J Cell Biol 146, 439–451.
Stein KK, Golden A (2015). The *C. elegans* eggshell. ed. WormBook, In: *C. elegans* Research Community. doi: 10.1895/wormbook.1.179.1.
Timmons L, Court DL, Fire A (2001). Ingestion of bacterially expressed dsRNAs can produce specific and potent genetic interference in *Caenorhabditis elegans*. Gene 263, 103–112.
Tse YC, Werner M, Longhini KM, Labbe JC, Goldstein B, Glotzer M (2012). RhoA activation during polarization and cytokinesis of the early *Caenorhabditis elegans* embryo is differentially dependent on NOP-1 and CYK-4. Mol Biol Cell 23, 4020–4031.
van der Voet M, Berends CW, Perreault A, Nguyen-Ngoc T, Gonczy P, Vidal M, Boxem M, van den Heuvel S (2009). NuMA-related LIN-5, ASPM-1, calmodulin and dynein promote meiotic spindle rotation independently of cortical LIN-5/GPR/Galpha. Nat Cell Biol 11, 269–277.
Yuce O, Piekny A, Glotzer M (2005). An ECT2-centralspindlin complex regulates the localization and function of RhoA. J Cell Biol 170, 571–582.
Zhang X, Ma C, Miller AL, Katbi HA, Bement WM, Liu XJ (2008). Polar body emission requires a RhoA contractile ring and Cdc42-mediated membrane protrusion. Dev Cell 15, 386–400.